DTU Library

Catalyst Degradation Under Potential Cycling as an Accelerated Stress Test for PBI-Based High-Temperature PEM Fuel Cells - Effect of Humidification

Søndergaard, Tonny; Cleemann, Lars Nilausen; Zhong, Lijie; Becker, Hans; Steenberg, Thomas; Hjuler, Hans Aage; Seerup, Larisa; Li, Qingfeng; Jensen, Jens Oluf

Catalyst Degradation Under Potential Cycling as an Accelerated Stress Test for PBI-Based High-Temperature PEM Fuel Cells—Effect of Humidification

Tonny Søndergaard[1], Lars Nilausen Cleemann[1], Lijie Zhong[1], Hans Becker[1], Thomas Steenberg[2], Hans Aage Hjuler[2], Larisa Seerup[1], Qingfeng Li[1], Jens Oluf Jensen[1],*

[a] Department of Energy Conversion and Storage, Technical University of Denmark, Kemitorvet 207, 2800 Kgs. Lyngby, Denmark
[b] Danish Power Systems Ltd., Egeskovvej 6C, 3490 Kvistgård, Denmark

Abstract

In the present work, high-temperature polymer electrolyte membrane fuel cells were subjected to accelerated stress tests of 30,000 potential cycles between 0.6 and 1.0 V at 160 °C (133 h cycling time). The effect that humidity has on the catalyst durability was studied by testing either with or without humidification of the nitrogen that was used as cathode gas during cycling segments. Pronounced degradation was seen from the polarization curves in both cases, though permanent only in the humidified case. In the unhumidified case, the performance loss was more or less recoverable following 24 h of operation at 200 mA cm^{-2}. A difference in degradation behavior was verified with electron microscopy, X-ray diffraction, and electrochemical impedance spectroscopy. The strong effect of humidification is explained by drying of the phosphoric acid that is in the catalyst layer(s) versus maintaining humidification of this region. Catalyst degradation due to platinum dissolution, transport of its ions, and eventual recrystallization is reduced when this portion of the acid dries out. Consequently, catalyst particles are only mildly affected by the potential cycling in the unhumidified case.

1. Introduction

Accelerated stress tests (ASTs) are desirable for studying the durability of fuel cells within a practical time frame and under well-defined conditions. Several kinds of electrode failure modes have been identified for high-temperature polymer electrolyte membrane fuel cells (HT-PEMFCs) with phosphoric acid-doped polybenzimidazole (PBI) electrolytes. As recently reviewed [1], electrode degradation is of particular interest for transient operation, which is circumstance for dynamic applications. The type of catalyst that is used almost exclusively for HT-PEMFCs is carbon-supported platinum (Pt/C), for which irreversible degradation can broadly be broken down to corrosion of either the carbon support or the catalyst metal [2]. Four mechanisms are generally considered to account for irreversible loss of the electrochemically active surface area (ECSA) [3–6]; these mechanisms are (1) carbon corrosion-induced agglomeration or detachment of platinum particles, (2) platinum particle coarsening by dissolution and recrystallization (Ostwald ripening), (3) platinum dissolution followed by recrystallization in the electrolyte phase, and (4) coalescence of platinum crystallites due to their mobility on the carbon surface.

Carbon corrosion to CO_2 can take place via reaction with water at potentials above 0.207 V versus SHE [7]. Though significant only at higher potential, this means that carbon corrosion may contribute to degradation of the cathode catalyst at normal fuel cell operation and that increasing water activity encourages the reaction. Because of insignificant platinum dissolution at low potentials, the adverse influence of Ostwald ripening will also be primarily affecting the cathode catalyst. This mechanism predicts preferential platinum dissolution from smaller particles and preferential recrystallization onto larger ones [4, 6, 8, 9]. Alternatively, as reviewed for low-temperature PEMFCs [5], platinum may recrystallize inside the electrolyte phase as (or onto) newly formed particles at a relative position determined by that of a hydrogen crossover front permeating from the anode. With progressive evolution of this mechanism, a band of platinum may form at the position of the said front [10–14]. In either case, loss of ECSA by dissolution and recrystallization of platinum will (1) occur in the presence of a solvent—the ion conducting phase, (2) be directly or indirectly potential dependent [9, 15], and (3) entail mobility of the platinum ions, a requisite for the particle coarsening and band formation mentioned above. Any catalyst degradation that is caused specifically by crystallite mobility on the carbon surface should be of comparable magnitude for either electrode under normal conditions [4].

2

To the authors' knowledge, only two references to platinum band formation have been made for HT-PEMFCs. Hartnig and Schmidt [16] showed band formation in the interface between the cathode and electrolyte after AST exposure with relatively frequent segments of current load being drawn (water production). Very recently, Rau et al. [17] showed the presence of a platinum band inside the membrane electrolyte of an HT-PEMFC after exposure to a load cycling AST with humidified anode gas. To date, it has not been made clear why platinum band formation has been largely absent in the HT-PEMFC literature compared to that for low-temperature PEMFCs—to the point where platinum dissolution into the electrolyte has been characterized as playing only a minor role during start-up/shutdown phases with potential excursions to 1.3 V [2]. However, as described for low-temperature PEMFCs, this conclusion may be inadvertently influenced by suppressed platinum dissolution on account of testing with unhumidified gasses [18–21].

AST protocols that focus on catalyst degradation will often assign nitrogen as the cathode gas since the use of oxidant will result in a large superimposed background current caused by the oxidation of hydrogen. This complicates distinction of the corrosion current from catalyst degradation. Moreover, accurate control of the potential may prove difficult over time when an oxidant is used as the cathode gas [22]. Since HT-PEMFCs exhibit no strong dependence on humidification, it is also customary to supply unhumidified gasses during their operation, even for AST evaluations, though periods with load being drawn seem common among most of the dynamic ones [2, 16, 17, 23–36]. Water should be present at the cathode during potential cycling, however, because this simulates the load cycling of fuel cells in dynamic use; while it might be assumed that the absence of current is of no consequence to potential cycling ASTs, the lack of current will entail the absence of water production. This is the focus of the present study, and we show that a potential cycling AST with unhumidified gasses is unreliable for catalyst durability evaluations. By adding water to the cathode gas during potential cycling, we then simulate the conditions of dynamic HT-PEMFC applications more closely and show that the results are comparably stable.

2. Experimental
2.1. Cell Preparation
Nonwoven carbon cloth was used as gas diffusion layer (GDL) onto which a microporous layer (MPL) had been applied (Freudenberg FCCT H23C2). The catalyst ink consisted of Pt/C (55.5–58.5 wt%, Johnson Matthey HiSPEC 9100) and of ethanol as dispersant, which was applied onto the MPL using a Sonotek ultrasonic spray robot. Each electrode had a platinum loading of approximately 1.5 mg cm^{-2}.

Membranes based on m-PBI with a thickness of 40 μm were fabricated by solution casting from a polymer solution in N,N-dimethylacetamide. After solvent removal, the membranes were equilibrated in phosphoric acid (85 wt% H_3PO_4) at room temperature for 24 h. Immediately after acid doping and removal of excess acid from the membrane surface, an acid doping level of 11.1–11.2 H_3PO_4 per polymer repeat unit was determined gravimetrically.

The membrane electrode assemblies (MEAs) were prepared by sandwiching a membrane in between two electrodes (5 × 5 cm^2) followed by hot pressing at 200 °C and 3.9 MPa for 3 min. Before hot pressing, frames of Kapton were introduced in the MEA to reinforce the membrane along the periphery of the electrodes, i.e., the nonreactive gas sealing area. The resulting MEAs had an active area of 21.2 cm^2.

2.2. Cell Assembly and Test Rig

The MEAs were tested as single cells. Gasses were supplied via graphite flow plates with a serpentine flow field (1 mm wide and 1 mm deep) that had 5 channels separated from one another by a spacing of 1 mm. Gas sealing of the cells was achieved with O-rings of fluoroelastomer (Viton). A layer of expanded flexible graphite (Papyex, Carbone Lorraine), with an uncompressed thickness of 1 mm, was used for gas sealing between the flow plates and the gold-coated current collectors. On the backside of the current collectors, a 1-mm-thick layer of a Viton was used for gas sealing as well as for electrical insulation from the end plates. Two aluminum end plates equipped with heating elements were used to clamp the MEA, flow plates, current collectors, and all of the seals. Clamping was done using two sets of 8 mm nuts and bolts in each of the four end plate corners and tightening these to a torque of 1 Nm.

The setpoint temperature was maintained in the end plates using Eurotherm temperature controllers. Gas flow rates were controlled using Brooks GF 40 thermal mass flow controllers. A Shimadzu LC-20AD parallel double microplunger type pump was used for internal gas humidification by supplying liquid water at a rate of approximately 12 µL min^{-1}, which was then evaporated in an in-house-designed evaporator before being directed into the fuel cell cathode chamber [37]. FuelCell testing software was used to program, control, and monitor the experiment. The experimental equipment that provided electrochemical control consisted of an 890e fuel cell test load, 885 potentiostat, and 880 frequency response analyzer from Scribner Associates Inc.

2.3. Experimental Protocol

The fuel cells were operated at 160 °C at all times. The experimental protocol was built up as a series of repeat sections, each of which was comprised of several individual segments. A minimum potential of 0.05 V was maintained throughout the entire protocol. As elaborated below, two different conditions were employed during cycling; the anode was supplied with hydrogen in both cases, while the cathode was supplied with either humidified or unhumidified nitrogen. Each segment of potential cycling was followed by a diagnostic sequence that consisted of electrochemical impedance spectroscopy (EIS) and polarization curve sampling, both measured with H_2/air. Hereafter, another set of EIS and polarization curve sampling were recorded but with H_2/O_2 instead. For stabilization, a conditioning period was enforced before commencing EIS measurements. A schematic illustration of a repeat section is shown in Fig. 1. To probe the beginning-of-life (BoL) cell characteristics, the entire protocol was initiated with a diagnostic sequence before any potential cycling had been carried out. All in all, diagnostic sequences were carried out after the following number of cycles 0, 10, 100, 1000, 3000, 5000, 10,000, 20,000, and 30,000. Furthermore, as a test of cell stability, an additional diagnostic sequence was conducted after the protocol had reached its conclusion, and steady-state operation for approximately 24 h at 200 mA cm^{-2} had been carried out. Execution of the experimental protocol from start to finish lasted nearly 9 days.

Square wave potential cycling was applied as stressor in this AST protocol with a potential hold time of 8 s per step both at 0.6 and at 1.0 V. In sequence from BoL, the potential cycling segments consisted of 10, 90, 900, 2000, 2000, 5000, 10,000, and 10,000 consecutive cycles. During cycling, the anode was supplied with 44 N mL min^{-1} of hydrogen, corresponding to lambda 1.5 at 200 mA cm^{-2}. In one of the two operation scenarios, the cathode was supplied with 170 N mL min^{-1} of unhumidified nitrogen (corresponding to lambda 2.4 at 200 mA cm^{-2} had it been replaced with air instead). In the other operation scenario, the cathode was supplied with internally humidified nitrogen of approximately the same total flow rate (170 N mL min^{-1}). The amount of water vapor in the nitrogen was approximately 15 N mL min^{-1}. This corresponds to a relative

4

humidity of 1.4% at the working temperature of 160 °C and equals the average water flow during operation for a cell of similar size when drawing a current of 200 mA cm^{-2}.

Cell conditioning prior to EIS measurements consisted of constant current operation at 200 mA cm^{-2} for 30 min. During conditioning, a hydrogen flow rate of 44 N mL min^{-1} was supplied to the anode and a flow rate of 170 N mL min^{-1} was supplied to the cathode, being either air or oxygen as matching the flow in the following EIS segment.

EIS was performed with a direct current bias of 200 mA cm^{-2} and with flow rates matching those of the preceding conditioning segment. In connection with EIS analyses, it should be mentioned that exhaust tubes were kept short enough to avoid water condensation and that cables were not moved during the entirety of the test period. EIS spectra were recorded by applying alternating current with amplitude corresponding to 7%$_{RMS}$ of the direct current bias. This translates to approximately $\pm$ 20 mA cm^{-2}. Fifteen frequencies were scanned per frequency decade from 7356 to 0.01 Hz, chosen so as to obtain impedance measurements at a phase angle of 0 for both high and low frequencies. The high-frequency impedance at a phase angle of 0 was taken as an estimate for the series resistance without correction for inductance. To determine what part of the EIS response from an operating fuel cell could not be attributed to the MEA, a high-frequency short circuit measurement was made of the empty setup at the operating temperature. This resistance amounted to approximately 7% of the BoL series resistance of the MEAs and has not been corrected for in the presented data because it includes contribution from an unrelated contact resistance, namely that between two flow plates, as introduced in the absence of an MEA.

Polarization curves were recorded from the open circuit voltage (OCV) and up to 1000 mA cm^{-2} by means of current step potentiometry. An initial stabilization time of 10 min at OCV was enforced before recording the first data point. For the remainder of the polarization curve, a 2-min stabilization time was enforced prior to recording of a data point. In sequence, the direct current characteristics were recorded with stepwise increases of 2.5, 25, and 50 mA cm^{-2} in the ranges from 0 to 25, 25 to 200, and 200 to 1000 mA cm^{-2}, respectively. Throughout sampling of H$_2$/air polarization curves, flow rates were applied with stoichiometries of approximately 1.6 and 2.4 for hydrogen and air, respectively. However, flow rate minima were imposed corresponding to 2% of the maximum set points for the hydrogen and air flow meters. Thus, a constant flow rate of approximately 17 N mL min^{-1} for hydrogen was supplied to the anode in the current range from 0 to 75 mA cm^{-2}, whereas a constant flow rate of approximately 52 N mL min^{-1} for air was supplied to the cathode in the range from 0 to 50 mA cm^{-2}. The H$_2$/O$_2$ polarization curves were recorded in an identical way, though with an oxygen flow rate in place of the values mentioned for air.

2.4. Postanalysis of the MEAs

Scanning electron microscopy (SEM) imaging and energy dispersive spectroscopy (EDS) analyses were carried out using a Zeiss EVO MA10 scanning electron microscope equipped with an X-Max 80-mm^2 INCA EDS system from Oxford Instruments. MEA cross sections for SEM were prepared by cutting with a scalpel followed by ion milling using a Hitachi E-3500. MEA micrographs were acquired immediately after ion milling.

Transmission electron microscopy (TEM) was performed using a Tecnai-T20-G2 electron microscope at 200 kV. TEM samples of catalyst were prepared from a small piece of each MEA (approximately 0.5×1 cm^2). The catalyst samples were attained by pealing back the GDL from the approximate region of the cathode flow inlet and, with a scalpel, scraping off the MPL onto which the catalyst adhered.

X-ray powder diffraction patterns were collected on a Rigaku Smartlab X-ray diffractometer (Cu-K$_\alpha$ radiation (45 kV, 200 mA)) with a step size of 0.02 in 2θ from 20° to 92° in 2θ using transmission geometry (focusing optics). Catalyst samples were collected by scraping off material from the polymer-electrode interface onto a piece of tape.

Acid-base titration was carried out on a circular piece of each MEA ($\varnothing = 1.26$ cm, 5.9% of the active area), prepared by die cutting. The samples were leached in 150 mL ultrapure water (Sartorius Arium pro UV, ASTM type 1 quality), which was stirred overnight. The solution was titrated with standardized 0.05 M NaOH (Sigma-Aldrich) using a Metrohm 808 Titrando titrator. Addition of titrant was paused when the solution pH approached that of the first equivalent point for phosphoric acid in order to accelerate leaching of residual acid. After waiting for at least 60 min, the titration was brought to conclusion with a pH endpoint of 4.9. Previous experience with this method has shown that 90–95% of the acid is extracted with adequate reproducibility; the standard deviations between acid measurements on individual cut-out samples from the same BoL MEAs were less than 1.3% of the average.

3. Results
3.1. Potential Cycling with Unhumidified Gasses

As practiced per usual for HT-PEMFCs, the first potential cycling test was performed using unhumidified gasses. The polarization curves for this test are presented in Fig. 2 and were recorded with gasses of either hydrogen and air or hydrogen and oxygen. The curves that were measured before cycling are indicated in the figure as BoL, whereas the curves measured after 3000, 10,000, and 30,000 cycles are indicated as 3k, 10k, and 30k, respectively. The final curves, designated as end-of-test (EoT) + 24 h, were measured after 30,000 cycles followed by operation at 200 mA cm^{-2} for 24 h.

The polarization curves are mildly depressed after 3000 cycles but are still mostly linear at high currents up to 1000 mA cm^{-2}. After 10,000 and 30,000 cycles, the curves show increasing degeneration with a limiting current behavior. For the polarizations with oxygen, the cell behaves qualitatively the same way as with air, although exhibiting the expected effects of a mitigated limiting current behavior (cf. the first section of the discussion part below) and an increased performance on account of oxygen gain [38, 39]. The last polarization curves are different, however. These were recorded in order to test the stability of the cell performance after cycling. Regardless of the oxygen partial pressure, these final polarization curves show almost complete recovery and, thus, that the degradation was reversible.

Nyquist plots of corresponding impedance spectra are shown in Fig. 3. Since the high-frequency intercept with the real axis (series resistance, shown in Fig. 7) is varying only a little over the course of the experiment compared to the overall polarization resistance, the change is considered comparably insignificant. The shape of the Nyquist plots when operated on pure oxygen is typical for this type of fuel cell, showing a minor high-frequency arc merged with a much larger intermediate-frequency arc. These two arcs are typically assigned to the anodic and cathodic charge transfer resistance, respectively [40]. With reference to the limiting current behavior that was seen for the polarization curves—even with pure oxygen—there are no clear signs of additional arcs or tails at low frequency in the EIS spectra recorded with pure oxygen (perhaps with a minor exception after 30,000 cycles). However, since the polarization curves measured with pure oxygen do not exhibit limiting current behavior at the direct current bias at which the EIS was measured, i.e., 200 mA cm^{-2}, there is agreement between the results.

The Nyquist plots for operation on air have the same features as those with oxygen, though with an additional low frequency semicircle that is visible already at BoL. This is usually interpreted as an indication of mass transport limitations [40]. However, since the polarization curves after 10,000 and 30,000 cycles are the only ones that show unequivocal limiting current behavior, the agreement with the polarization curves is not entirely straightforward in this regard. Perhaps, this can be explained by better resolution with the EIS technique at the particular operating point. Both for air and for oxygen measurements, the intermediate-frequency arc grows concomitant with cycling and it returns partly to the size observed at BoL after 30,000 cycles when followed by operation at 200 mA cm^{-2} for 24 h. The small high-frequency anodic arc might, in both cases, have grown ever so slightly at EoT as compared to at BoL, indicating some anodic degradation as well.

3.2. Potential Cycling with Humidified Cathode Gas

The potential cycling experiment was repeated on another cell using humidified nitrogen during the cycling periods. The resulting polarization curves are shown in Fig. 4. Again, pronounced degradation is evident concomitant with cycling. Now, however, the stability test after 30,000 cycles shows no recovery subsequent to operation at 200 mA cm^{-2} for 24 h. Thus, the degradation is irreversible in this case. Another difference is that the polarization curves are significantly affected in the low current region, which pertains to activation overpotential. The resulting effect is that the curves are shifted to lower voltages in a more or less parallel manner. Also for this experiment, the limiting current is seen to decrease concomitant with cycling, while the OCV (Fig. 6), which was practically unchanged in the unhumidified case, has decreased about 200 mV during the humidified experiment.

More so than for the EIS measurements obtained in the unhumidified case, the Nyquist plots show practically unchanged series resistance (Fig. 7) whereas an increase of the polarization resistance concomitant with cycling is common among both experiments; see Fig. 5. On the other hand, like the polarization curves, the final EIS measurements in the humidified case showed no recovery and are coinciding with the ones recorded immediately after 30,000 cycles. It is possible that the high-frequency anodic arc has grown, though it is difficult to see this clearly. Comparing the EIS measurements in the two cases after any given number of cycles (Fig. 3 vs. Fig. 5), the air measurements suggest that the most significant increase of the polarization resistance occurs in the unhumidified case. However, the pure oxygen measurements suggest this trend for the humidified case instead.

3.3. OCV Comparison

As a supplement to the polarization curves shown in Figs. 2 and 4, comparison of the OCV measurements from all recorded polarization curves is shown in Fig. 6. In total, 20 polarization curves were measured for each test, i.e., 10 with H_2/air and another 10 with H_2/O_2. There is a significant decrease of the OCV over the course of the experiment only in the humidified case. The slight increase of the OCV during the first 20 to 50 h can to some extent reflect the process of attaining equilibrium during the dynamics of the activation process, often referred to as break-in for HT-PEMFCs. However, the main reason is most likely that the acid in the membrane is becoming increasingly dehydrated (cf. Fig. 7), resulting in a lowering of the gas crossover rate. Gas crossover is accepted as being a main influencing factor on the OCV due to the formation of a mixed potential. A partial drying is supported by an almost equivalent lowering of the OCV after

24 h of posttest normal operation. As expected from the evident oxygen gain seen in Figs. 2 and 4, the OCV measurements for the same cell were all lower with H_2/air than with H_2/O_2.

3.4. Comparison of the Series Resistance
Similar to the OCV comparison above, a supplementary comparison of the series resistance from all EIS spectra is shown in Fig. 7. Again, a total of 20 measurements have been made for each test, i.e., 10 with H_2/air and another 10 with H_2/O_2. As a general trend, the change in series resistance is decreasing in the humidified case, though the overall change from BoL to EoT is relatively minor. In the unhumidified case, the change in series resistance is increasing over the course of the experiment, more so for the measurements with H_2/air than for the ones with H_2/O_2. As alluded to by the OCV measurements, this suggests that the electrolyte is becoming partly dehydrated over the course of the experiment, whereas the observed increase of the series resistance is almost completely reversed after 24 h of posttest normal operation.

3.4. Post Analysis of the MEAs
The average platinum particle size was examined by TEM for the pristine catalyst and for the MEA electrodes after cycling; see micrographs in Fig. 8 and pertaining size estimations in Table 1. Each of the average size estimations with TEM is based on three different TEM images of which only one is shown. It can be seen that the commercial Pt/C catalyst is quite homogeneous with an average diameter of 3.5 nm (Fig. 8a). After testing, the anode catalyst shows slight degradation in that the platinum particle size has increased to an average of 4.5 nm for both cells, regardless of whether the cathode gas was humidified (Fig. 8c) or not (Fig. 8b). On the other hand, the cathode catalyst shows disparate particle growth to an average of 6 nm in the unhumidified case (Fig. 8d) compared to 10 nm in the humidified case (Fig. 8e).

For verification, the average platinum particle sizes were also estimated from peak broadening of X-ray diffraction data by the use of the Scherrer method. These estimations are shown in Table 1 in brackets. Due to uncertainty with the applied methods, the platinum particle size estimations do not coincide completely. The discrepancy is largest for the humidified cathode. The larger crystallite size measurement by the Scherrer method can possibly have been influenced by part of a Pt band, which is shown below in Fig. 9. The tendency of the growth is clearly comparable between the two methods, however.

Cross sections of the cells after 30,000 cycles were examined by SEM as shown in Fig. 9 with EDS line scans for platinum superimposed onto the micrographs. It is evident from the atom number contrast (brighter signal for heavier elements, i.e., platinum) that a platinum band is formed in the interface between the membrane and the cathode electrode only in the humidified case. Furthermore, it is only in this case that the cathode appears slightly darker than the anode.

Finally, the acid content after testing was determined by titration; see Table 2. Since the membranes of the tested MEAs were from two different production batches, the reference acid content at BoL has been determined for them both. There was no significant difference in the amount of acid that was lost from the two cells, though the overall acid loss in itself was significant.

4. Discussion
The experiments clearly show that water is crucial for the intended effect of the AST, which is to assess the cathode catalyst resistance toward loss of ECSA on account of platinum particle growth and platinum band formation. Two questions then arise: why is the permanent degradation almost

insignificant in the unhumidified case and why is an apparent (reversible) degradation detected in the unhumidified case in the first place?

4.1. Reasons for Limiting Current Behavior

Limiting current behavior occurs when the reaction rate is becoming restricted and is usually seen at high currents since this is tantamount to a fast reaction rate. The behavior will look the same whether the restriction is caused by (1) insufficient active catalyst sites (or ECSA) for reactants to adsorb onto, (2) insufficient activity of reactant(s) (usually local partial pressure due to hindered high-rate transport) for adequately sustained coverage of the active catalyst sites, or (3) a limitation for a given reaction rate constant, e.g., the rate at which the reactant(s) can actually adsorb onto the available active sites of the catalyst. In relation to the experiments presented here, it seems reasonable to presume that there is no change to the reaction rate constants over the course of either experiment. Thus, any aggravation of the limiting current should be ascribable either to a loss of active catalytic sites or to a transport hindrance of the reactant(s).

4.2. The Humidified Case

In the humidified case, the polarization curves take shape concomitant with cycling as is expected for progressively decreasing ECSA. As was just mentioned, the aggravation of the limiting current can, in fact, be explained by such a progressive restriction. Furthermore, a loss of ECSA will lead to a reduction of the exchange current density with respect to the geometric electrode area. In turn, the activation polarization becomes stronger at any geometric current density, so the polarization curves shift to progressively lower voltage as predicted by the Butler-Volmer equation. The decreasing OCV can also be ascribed to this effect; stronger polarization at any geometric current density includes that which is required of the cathode to oxidize crossover hydrogen at OCV. Notice in this regard that the linear slope of the polarization curves at intermediate current densities, which is dominated by series resistance, remains mostly unchanged. Knowing that the ion conductivity of phosphoric acid depends strongly on its water content, this suggests that there is only limited change to the hydration level of the bulk electrolyte itself at the time of the measurements [41, 42]. The small OCV depression discussed above, however, does indicate some dehydration of the bulk electrolyte, but apparently not enough to affect the series resistance significantly. The overall interpretation of the polarization curves agrees with the EIS spectra; the polarization resistance, legible primarily from the medium-frequency arc (kinetic resistance) and low-frequency arc (rate limitation), is progressively increasing, whereas the series resistance remains mostly unchanged.

The significant platinum particle growth and the identification of a platinum band suggest that the loss of ECSA is caused by a loss of platinum surface. Furthermore, it suggests that potential cycling does incite degradation of the cathode catalyst in the humidified case via platinum dissolution and recrystallization. Another indication of this mechanism was a small corrosion current of a few milliamperes per square centimeter (not shown), which changed direction as the voltage was shifted back and forth between 0.6 and 1.0 V. The difference in atom number contrast between the anode and the cathode can be explained by there being less platinum in the cathode catalyst layer, which is an expected consequence of its transport to form a band at the interface between the membrane and the cathode. Attempts at quantifying the ECSA loss could have been made, e.g., by comparing the BoL and EoT characteristics using cyclic voltammetry. While this is a routine analysis for low-temperature PEMFCs, the higher operational temperature and strong adsorption of phosphate anions for HT-PEMFCs makes it unfeasible at the working temperature

to quantitatively determine the platinum surface area by means of hydrogen underpotential deposition and makes for nontrivial determination by the alternative CO adsorption [43].

4.3. Formation of the Platinum Band

As mentioned in the Introduction, platinum dissolving from the cathode is believed to recrystallize upon reduction by crossover hydrogen permeating from the anode [15, 44]. Any gradient of the potential across the electrolyte phase should encourage platinum transport via migration as well. However, little is known about the state of the platinum ions (complexes, charge, etc.) [45]. With progressive evolution of the platinum recrystallization as (or onto) newly formed particles, a band of platinum particles may eventually form at a banding zone where the molar flux of crossover hydrogen permeating from the anode equals twice the molar flux of crossover oxygen permeating from the cathode [10–13]. This position will shift toward the anode with decreasing anode-side hydrogen partial pressure and/or with increasing cathode-side oxygen partial pressure due to imposed change of the crossover flux [12–14, 46]. Eventually, the two gas crossover fronts will become mutually arrested at the particular location of the banding zone since they will be used up stoichiometrically to form water, which is catalyzed by the precipitated platinum. In our case, the reducing front of crossover hydrogen is expected to make it all the way to the cathode since there is no crossover oxygen available during the H_2/N_2 operation. Thus, the specific position of the platinum band in the interface between the membrane and the cathode is to be expected.

4.4. Rehydration in the Unhumidified Case

The limiting current behavior is reversible only in the unhumidified case. This indicates, quite convincingly, that the reversibility is due to acid rehydration during the final 24 h of normal service when water is produced. It is interesting to note that the series resistance from the EIS spectra over the course of both experiments remains largely unaffected in comparison to the change in polarization resistance, suggesting that the drying of the bulk electrolyte itself is of secondary importance at the time of the measurements. However, the OCV measurements do indicate some initial change in gas permeability in agreement with the change in series resistance when cycling with unhumidified gasses followed by reversal of the effect after the 24 h of normal service. Indeed, there should be time for some drying to occur during the cycling segments; 2000, 5000, and 10,000 cycles correspond to 9, 22, and 44 h, respectively. Apparently, some drying of the bulk electrolyte does take place, but not to an extent that severely changes the area-specific series resistance, at least not in comparison to the observed change in polarization resistance. Thus, the pronounced effect of drying is ascribed mainly to a serious dehydration of the catalyst layer(s).

The effect of drying is less pronounced for the oxygen measurements, because these were made after the air measurements and were, therefore, preceded by a longer period of water production (rehydration). The additional time with water production (a second conditioning period, a polarization curve with air, and an EIS measurement with air) amounts to approximately 3 h compared to the 30 min of conditioning prior to the EIS measurement with air. This can explain the disparate observation after any given number of cycles that the most pronounced increase of the polarization resistance occurs for the humidified case according to the oxygen measurements but occurs for the unhumidified case according to the air measurements.

Obviously, the enforced conditioning period was insufficient for establishing a reference hydration state. Furthermore, it is apparent that the periods during which current is drawn are too short or infrequent to allow for adequate rehydration. On the other hand, the results of the final diagnostic sequence closely resemble those of the first in the unhumidified case. This suggests that

24 h of normal service might be enough time to allow for complete recovery/rehydration, save for what is believed to be minor permanent degradation (cf. Fig. 8 and Table 1). However, this residual degradation in the electrochemical tests might, at least in part, be a lingering effect of drying, which has not been completely mended even after 24 h of normal service.

4.5. The Role of Water in the Loss of Platinum Surface Area

The water activity may affect the platinum dissolution by changing the chemical environment as well as the ion conductivity of the phosphoric acid. First off, several of the proposed mechanisms by which platinum dissolution can take place involve formation of an intermediate oxide through reaction with water [15, 47]. With low water activity, these pathways may be restricted. Furthermore, drying out of phosphoric acid in the catalyst layer(s) will reduce the ion conductivity [41, 42]. In turn, this may restrict the directly potential-dependent (electrochemical) platinum dissolution mechanisms as these necessitate transport of ions within the cathode catalyst layer to balance the electric corrosion current that is generated when platinum dissolves and recrystallizes.

Compared to LT-PEMFCs, the presence of phosphoric acid adds to the intricacy because platinum ions can form complexes with phosphate species [48, 49]. If the phosphoric acid in the cathode catalyst layer is dehydrated and partly condensed, platinum compounds of pyro- and metaphosphates may form in favor of platinum orthophosphate compounds. In turn, the transport rate of platinum will probably slow down due to higher viscosity of the dehydrated solvent as well as lower mobility of these bulkier complexes.

Even for steady-state operation, slight growth of the platinum particles on either electrode is to be expected. Thus, it is of no surprise that the XRD and TEM results (Table 1) reveal some platinum particle growth on the anode for both cells. However, the effect of potential cycling as a trigger for the loss of ECSA due to platinum dissolution and recrystallization is much less severe in the unhumidified case. This was evidenced by the comparable platinum particle growth between the anode and the cathode as well as the absence of a platinum band for this cell. The resulting effect is that there is no shift of the polarization curves concomitant with cycling because the exchange current is largely unaffected. Some minor irreversible degradation is understandable, however, both because it takes a certain amount of time before the dry state is established but also because the protective effect from drying is not absolute. Particularly at the beginning of each cycling segment, irreversible degradation may occur even in the unhumidified case because water has been produced immediately beforehand.

4.6. The Role of Water in the Apparent Degradation

Several avenues have been explored to explain the apparent (reversible) degradation in the unhumidified case, i.e., the progressively aggravated limiting current. As was just mentioned, it is clear that a loss of catalytic sites cannot be the reason for the rate limitation in this case. Furthermore, knowing that the predominant mechanism for carbon corrosion involves water, it seems unreasonable to ascribe it to gas transport limitation following corrosion-induced densification of the cathode. Besides, any degradation that is caused by a loss of catalytic sites or by carbon corrosion should be irreversible, whereas reversibility was, in fact, observed. On this basis, two plausible explanations are suggested for the apparent degradation in the unhumidified case, both of which can be traced back to the low water activity and drying out of the phosphoric acid in the catalyst layer(s).

It is often assumed that the catalyst particles are covered by a film of phosphoric acid, a conjecture that is supported by the high affinity that phosphate ions have to the platinum surface

[50, 51]. If so, oxygen must penetrate a film of acid in order to reach the catalytic sites of the cathode. As the acid in the cathode catalyst layer is drying out, this may give rise to progressive transport limitation based on the inference that oxygen diffusion and solubility is reduced [52–56].

The other explanation is related to the reduced ion conductivity of the acid in the catalyst layer(s) when it dries out. A larger fraction of the overall electromotoric force will then be spent on proton transport. Naturally, this voltage drop is locally ohmic. However, it is not evenly distributed over the width of the catalyst layer(s); the farther from the membrane, the higher the voltage drop. Putting it in another way, with low ion conductivity in the catalyst layer(s), it may be that the catalyst closest to the membrane is the only part with sufficient electrochemical connection. Consequently, at a distance from the membrane, the current load will be lower, and the voltage that is available for overcoming the activation barrier will be lower as well. This may give rise to reduced catalyst utilization at remote sites of the catalyst layer(s) as well as a higher current load on the sites that are closer to the membrane. Indeed, a higher load on fewer active sites can be the cause of rate limitation as already discussed. Notice, however, that this explanation suggests reduction of the catalyst utilization only at higher currents. Thus, the polarization curve should still remain more or less unaffected at low current since Ohm's law will then dictate only a small voltage drop. Therefore, no shift of the polarization curves to lower voltage is expected on this account.

4.7. Acid Loss
Since the amount of acid loss between the cells is comparable, it seems reasonable to conclude that humidification does not introduce noteworthy degradation that is pertinent in this regard. This could have been a possible concern owing to a proposed mechanism of acid loss via steam distillation [25]. Furthermore, the acid loss via evaporation should be minimal since each experiment lasted less than 2 weeks. This agrees with the EIS measurements and, to a lesser extent, with the polarization curves; over the course of the experiment, a significant and permanent change is seen neither to the series resistance in the Nyquist plots nor to the slope of the linear region of the polarization curves (most obvious from the BoL and EoT curves measured with oxygen). On the other hand, a significant acid loss was identified for both cells (Table 2). Thus, the acid loss is presumed to have occurred by other means, e.g., in connection with start-up; clamping enacts a compressive force to a cell, which promotes acid squeeze-out, particularly during the initial heating where structural integrity of the electrolyte is compromised on account of softening. This effect is similar to that which occurs during MEA hot pressing, and hot pressing has been shown to account for an acid loss of approximately 29% from an MEA based on a membrane produced via the pyrophosphoric acid (PPA) process when followed by a subsequent heat treatment at 160 °C for 24 h [25].

5. Conclusions
Humidification strongly influences the effect that potential cycling has as an AST stressor in the evaluation of platinum catalyst durability; cycling the cathode of an HT-PEMFC at 160 °C between 0.6 and 1.0 V in an atmosphere of either humidified or unhumidified nitrogen will lead to vastly different degradation behavior. Regardless of humidification, polarization curves show aggravated limiting current behavior over the course of the experiment, though largely reversible only in the unhumidified case. On the other hand, it is only in the humidified case that the polarization curves exhibit a drop in OCV and a parallel shift to lower voltage. These observations in the humidified case are ascribed to a decrease of the exchange current concomitant with cycling

because of reduced ECSA when active platinum sites are lost on account of progressive platinum dissolution, transport, and recrystallization. This interpretation agrees with the EIS spectra, the XRD and TEM measurements of increased platinum particle size, as well as with the identification of a platinum band. Apart from the aggravation of the limiting current, all of these observations were either insignificant or not detectable in the unhumidified case.

That the loss of platinum surface area is less in the unhumidified case is explained by a protective effect of dehydration; as the phosphoric acid in the catalyst layer(s) dries out and polymerizes, there may be a restriction of the platinum dissolution mechanisms that necessitate ion conductivity and/or that involve reaction with water. Furthermore, the transport rate of the dissolved platinum may be slower due to higher viscosity of the dehydrated solvent and because of lower mobility of platinum phosphate complexes if these are formed with the bulkier ligands of polymerized acid. The performance loss in the unhumidified case, i.e., aggravation of the limiting current behavior, is ascribed to rate limitation in the dried out catalyst layer(s). The proposed reasons for this are reduced oxygen diffusion and solubility in the acid film that covers the cathode catalyst and/or reduced ion conductivity in the catalyst layer(s), rendering the catalyst sites furthest from the membrane unavailable at high current.

Without humidification or frequent periods wherein current is drawn to maintain humidity, potential cycling ASTs will most likely be unreliable for evaluating the durability of HT-PEMFC cathode electrocatalysts. The apparent degradation in the unhumidified case might be misinterpreted as a result of platinum surface area loss. Conversely, if the catalyst layer has dried out during cycling but is allowed to rehydrate prior to performance diagnostics, say in connection with a cell conditioning period where current is drawn, then a different erroneous conclusion might be inferred with an invalid claim of excellent catalyst durability. Using humidified cathode gas, however, it is possible to incite significant and permanent degradation of the cathode catalyst. With no notable aggravation of acid loss during the testing period, this AST should be applicable also for HT-PEMFCs. It may be possible to utilize the protective effect of drying as an operation strategy in order to mitigate platinum dissolution when a particular mode of operation dictates potential excursions to high values.

6. Funding Information

7. References

1. M.T.D. Jakobsen, J.O. Jensen, L.N. Cleemann, Q. Li, in *High Temperature Polymer Electrolyte Membrane Fuel Cells: Approaches, Status and Perspectives*, ed. by Q. Li, D. Aili, H.A. Hjuler, J.O. Jensen. (Springer, Cham, 2016), pp. 487–509
2. T.J. Schmidt, in *Polymer Electrolyte Fuel Cell Durability*, ed. by F.N. Büchi, M. Inaba, T.J. Schmidt. (Springer, New York, 2009), pp. 199–221
3. P.J. Ferreira, G.J. la O', Y. Shao-Horn, D. Morgan, R. Makharia, S. Kocha, H.A. Gasteiger, J. Electrochem. Soc. 152, A2256-A2271 (2005)
4. Y. Shao-Horn, W.C. Sheng, S. Chen, P.J. Ferreira, E.F. Holby, D. Morgan, Top. Catal. 46, 285–305 (2007)
5. J. Li, in *PEM Fuel Cell Electrocatalysts and Catalyst Layers: Fundamentals and Applications*, ed. by J. Zhang. (Springer, London, 2008), pp. 1041–1094

6. K. Sasaki, M. Shao, R. Adzic, in *Polymer Electrolyte Fuel Cell Durability*, ed. by F.N. Büchi, M. Inaba, T.J. Schmidt. (Springer, New York, 2009), pp. 7–27

7. K. Kinoshita, *Carbon: Electrochemical and Physiochemical Properties* (Wiley, New York, 1988), pp. 316–334

8. A.V. Virkar, Y. Zhou, J. Electrochem. Soc. 154, B540–B547 (2007)

9. M.J. Eslamibidgoli, J. Huang, T. Kadyk, A. Malek, M. Eikerling, Nano Energy 29, 334–361 (2016)

10. V. Atrazhev, S.F. Burlatsky, N.E. Cipollini, D.A. Condit, N. Erikhman, ECS Trans. 1, 239–246 (2006)

11. A. Ohma, S. Suga, S. Yamamoto, K. Shinohara, ECS Trans. 3, 519–529 (2006)

12. W. Bi, G.E. Gray, T.F. Fuller, Electrochem. Solid State Lett. 10, B101–B104 (2007)

13. J. Zhang, B.A. Litteer, W. Gu, H. Liu, H.A. Gasteiger, J. Electrochem. Soc. 154, B1006–B1011 (2007)

14. L. Kim, C.G. Chung, Y.W. Sung, J.S. Chung, J. Power Sources 183, 524–532 (2008)

15. S. Cherevko, N. Kulyk, K.J.J. Mayrhofer, Nano Energy 29, 275–298 (2016)

16. C. Hartnig, T.J. Schmidt, J. Power Sources 196, 5564–5572 (2011)

17. M. Rau, A. Niedergesäß, C. Cremers, S. Alfaro, T. Steenberg, H.A. Hjuler, Fuel Cells 16, 577–583 (2016)

18. R.L. Borup, J.R. Davey, F.H. Garzon, D.L. Wood, M.A. Inbody, J. Power Sources 163, 76–81 (2006)

19. M. Uchimura, S. Sugawara, Y. Suzuki, J. Zhang, S.S. Kocha, ECS Trans. 16, 225–234 (2008)

20. W. Bi, Q. Sun, Y. Deng, T.F. Fuller, Electrochim. Acta 54, 1826–1833 (2009)

21. F.T. Wagner, S.G. Yan, P.T. Yu, in *Handbook of Fuel Cells: Fundamentals, Technology and Applications—Volume 5: Advances in Electrocatalysis, Materials, Diagnostics and Durability*, ed. by W. Vielstich, H. Yokokawa, H.A. Gasteiger (Wiley, Weinheim, 2009), p. 250–264

22. S.S. Kocha, in *Polymer Electrolyte Fuel Cell Degradation*, ed. by M.M. Mench, E.C. Kumbur, T.N. Veziroğlu. (Academic, Oxford, 2012), pp. 89–214

23. Y. Zhai, H. Zhang, D. Xing, Z.-G. Shao, J. Power Sources 164, 126–133 (2007)

24. T.J. Schmidt, J. Baurmeister, J. Power Sources 176, 428–434 (2008)

25. S. Yu, L. Xiao, B.C. Benicewicz, Fuel Cells 8, 165–174 (2008)

26. P. Moçotéguy, B. Ludwig, J. Scholta, Y. Nedellec, D.J. Jones, J. Rozière, Fuel Cells 10, 299–331 (2010)

27. M.R. Berber, T. Fujigaya, K. Sasaki, N. Nakashima, Sci Rep 3, 1764 (2013)

28. L.N. Cleemann, F. Buazar, Q. Li, J.O. Jensen, C. Pan, T. Steenberg, S. Dai, N.J. Bjerrum, Fuel Cells 13, 822–831 (2013)

29. M. Rastedt, D. Schonvogel, P. Wagner, ECS Trans. 64, 741–753 (2014)

30. N. Pilinski, M. Rastedt, P. Wagner, ECS Trans. 69, 323–335 (2015)

31. F.J. Pinar, N. Pilinski, M. Rastedt, P. Wagner, Int. J. Hydrog. Energy 40, 5432–5438 (2015)

32. F. Zhou, S.J. Andreasen, S.K. Kær, D. Yu, Int. J. Hydrog. Energy 40, 2833–2839 (2015)

33. F.J. Pinar, M. Rastedt, N. Pilinski, P. Wagner, Int. J. Hydrog. Energy 41, 19463–19474 (2016)

34. M. Rastedt, F.J. Pinar, N. Pilinski, A. Dyck, P. Wagner, ECS Trans. 75, 455–469 (2016)

35. D. Schonvogel, M. Rastedt, P. Wagner, M. Wark, A. Dyck, Fuel Cells 16, 480–489 (2016)

36. R. Taccani, T. Chinese, M. Boaro, Int. J. Hydrog. Energy 42, 1875–1883 (2017)

37. A. Vassiliev, High Temperature PEM Fuel Cells and Organic Fuels. (PhD thesis, Department of Energy Conversion and Storage, Technical University of Denmark, 2014)

38. M. Prasanna, H.Y. Ha, E.A. Cho, S.-A. Hong, I.-H. Oh, J. Power Sources 137, 1–8 (2004)
39. K. O'Neil, J.P. Meyers, R.M. Darling, M.L. Perry, Int. J. Hydrog. Energy 37, 373–382 (2012)
40. X.-Z. Yuan, S. Chaojie, W. Haijiang, Z. Jiujun, *Electrochemical Impedance Spectroscopy in PEM Fuel Cells: Fundamentals and Applications* (Springer, London, 2010), pp. 193–262
41. C. Korte, F. Conti, J. Wackerl, W. Lehnert, in *High Temperature Polymer Electrolyte Membrane Fuel Cells: Approaches, Status and Perspectives*, ed. by Q. Li, D. Aili, H.A. Hjuler, J.O. Jensen. (Springer, Cham, 2016), pp. 169–194
42. J.-P. Melchior, K.-D. Kreuer, J. Maier, Phys. Chem. Chem. Phys. 19, 587–600 (2017)
43. T. Engl, K.E. Waltar, L. Gubler, T.J. Schmidt, J. Electrochem. Soc. 161, F500–F505 (2014)
44. R.M. Darling, J.P. Meyers, J. Electrochem. Soc. 152, A242–A247 (2005)
45. M.P. Rodgers, L.J. Bonville, H.R. Kunz, D.K. Slattery, J.M. Fenton, Chem. Rev. 112, 6075–6103 (2012)
46. M.J. Eslamibidgoli, P.-É.A. Melchy, M.H. Eikerling, Phys. Chem. Chem. Phys. 17, 9802–9811 (2015)
47. R. Borup, J. Meyers, B. Pivovar, Y.S. Kim, R. Mukundan, N. Garland, D. Myers, M. Wilson, F. Garzon, D. Wood, P. Zelenay, K. More, K. Stroh, T. Zawodzinski, J. Boncella, J.E. McGrath, M. Inaba, K. Miyatake, M. Hori, K. Ota, Z. Ogumi, S. Miyata, A. Nishikata, Z. Siroma, Y. Uchimoto, K. Yasuda, K.-I. Kimijima, N. Iwashita, Chem. Rev. 107, 3904–3951 (2007)
48. P. Bindra, S.J. Clouser, E. Yeager, J. Electrochem. Soc. 126, 1631–1632 (1979)
49. K. Mitsuda, H. Shiota, T. Murahashi, Corrosion 46, 628–633 (1990)
50. Q. Li, X. Gang, H.A. Hjuler, R.W. Berg, N.J. Bjerrum, J. Electrochem. Soc. 141, 3114–3119 (1994)
51. R. Zeis, Beilstein J. Nanotechnol. 6, 68–83 (2015)
52. K.E. Gubbins, R.D. Walker Jr., J. Electrochem. Soc. 112, 469–471 (1965)
53. K. Klinedinst, J.A.S. Bett, J. Macdonald, P. Stonehart, J. Electroanal. Chem. Interfacial Electrochem. 57, 281–289 (1974)
54. F. Gan, D.-T. Chin, J. Appl. Electrochem. 23, 452–455 (1993)
55. Z. Liu, J.S. Wainright, M.H. Litt, R.F. Savinell, Electrochim. Acta 51, 3914–3923 (2006)
56. M. Fleige, K. Holst-Olesen, G.K.H. Wiberg, M. Arenz, Electrochim. Acta 209, 399–406 (2016)
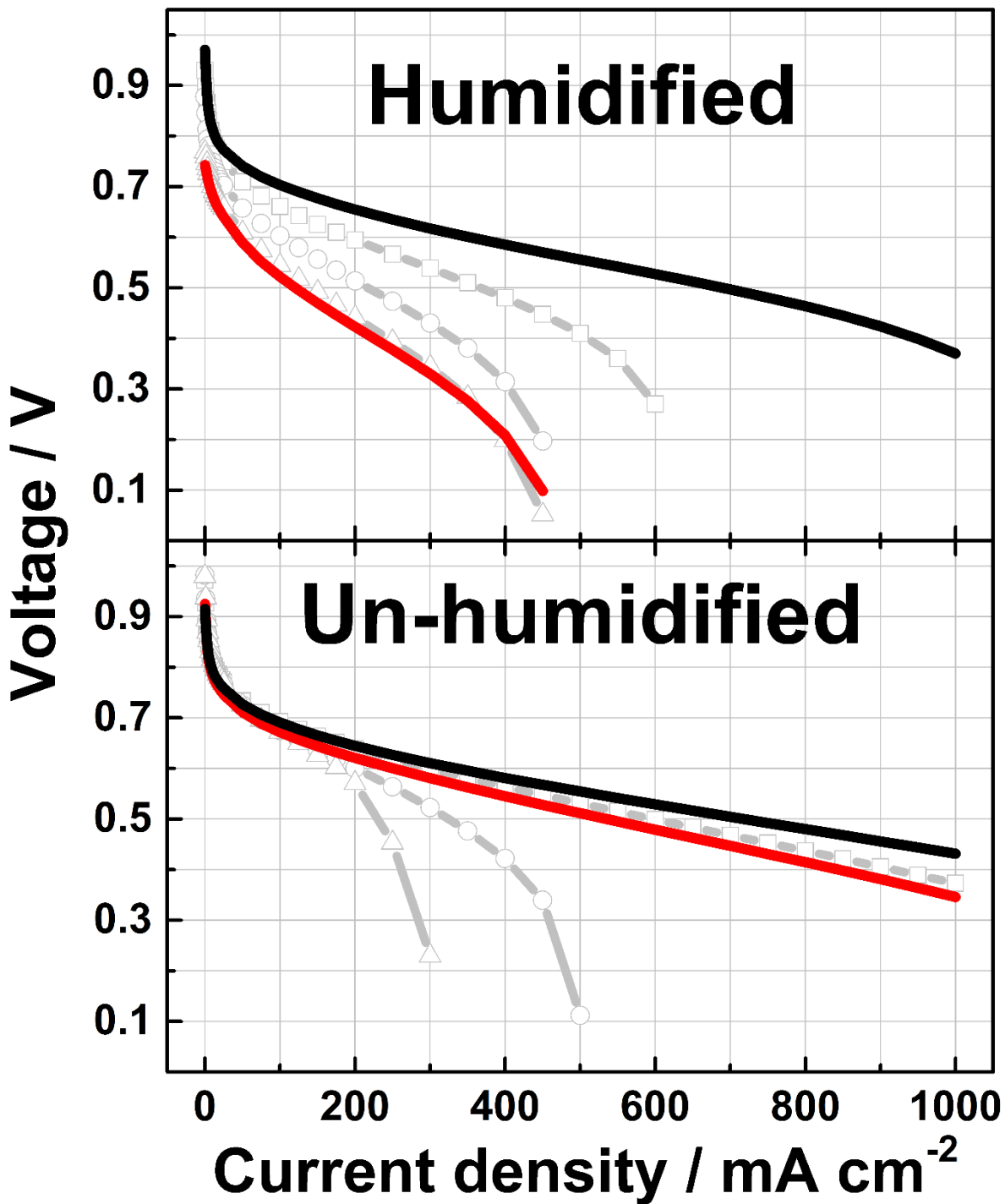
Table 1 Average platinum particle size estimations from the TEM histograms shown in Fig. 8 for the pristine catalyst and for the electrocatalysts after potential cycling with either H_2/N_2 (unhumidified) or with H_2/N_2 (humidified). The numbers in brackets represent the average particle sizes as estimated by X-ray diffraction using the Scherrer method

	Anode, nm	Cathode, nm
BoL	3.5 (4.7)	
Unhumidified	4.5 (6.1)	6 (6.6)
Humidified	4.5 (6.8)	10 (20.6)

Table 2 Area-specific acid content of MEAs after cycling (EoT) with H_2/N_2 (unhumidified) or with H_2/N_2 (humidified). The comparison is relative to the acid content of reference MEAs from corresponding batches (BoL)

	BoL, μmol cm^{-2}	EoT, μmol cm^{-2}	Loss, %
Unhumidified	152	120	21
Humidified	149	114	23

Fig. 1 Schematic illustration of the diagnostic sequence in between two segments of AST cycling. The insert shows the applied square wave cycling pattern
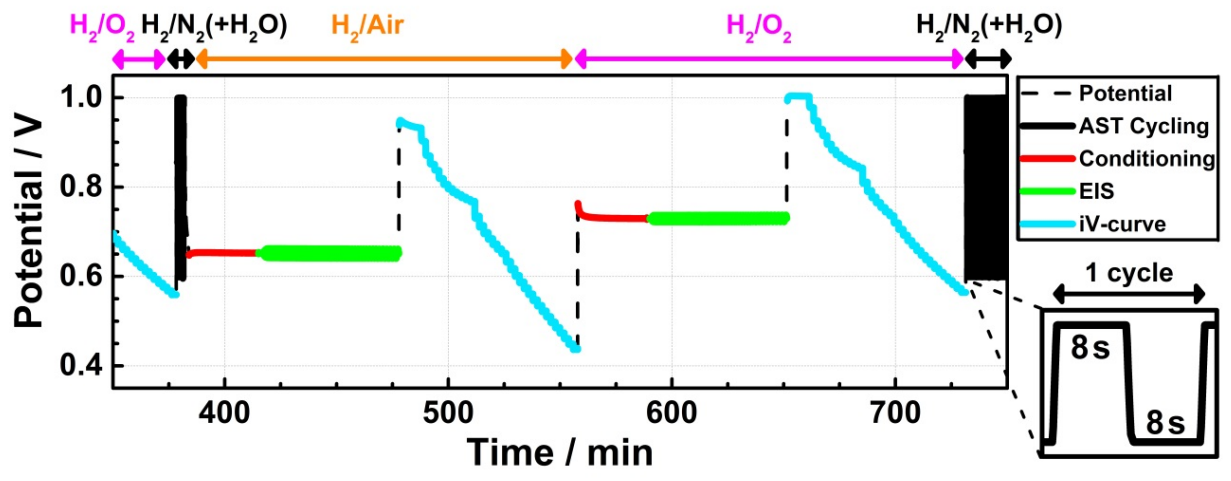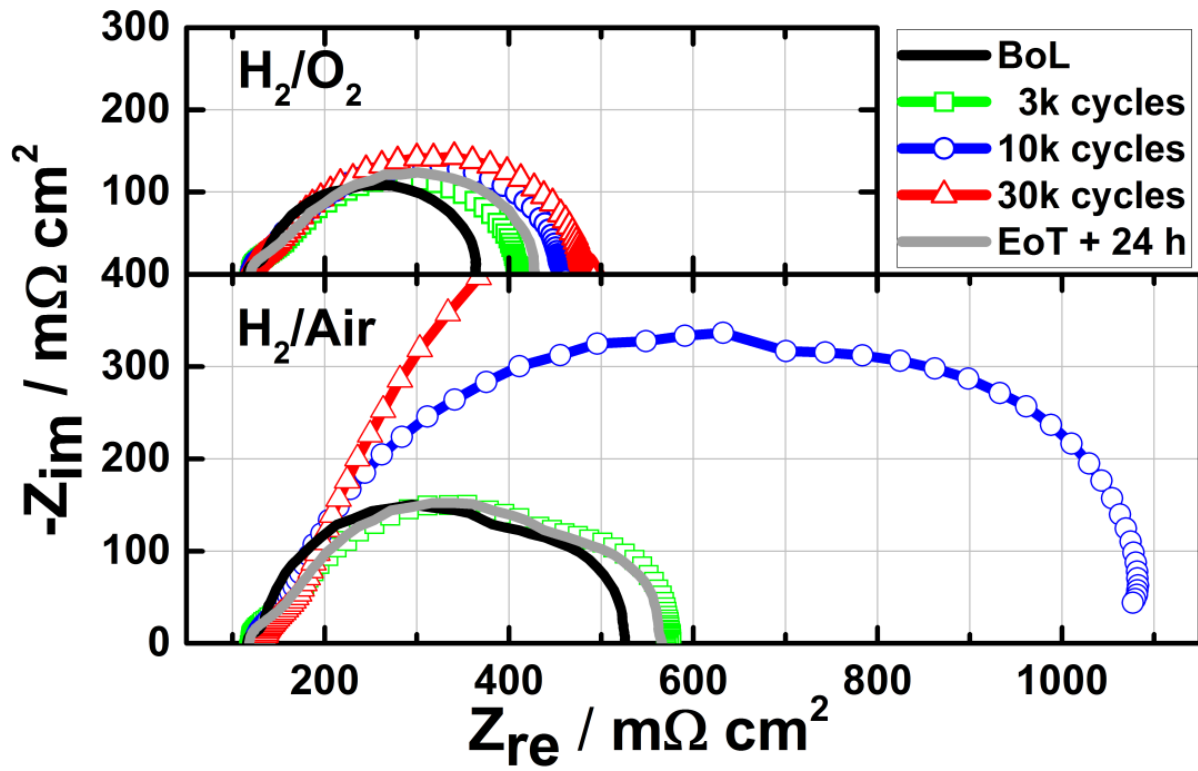
Fig. 2 Polarization characteristics at BoL, after the specified number of cycles with H_2/N_2 (unhumidified), and also after 30,000 cycles followed by 24 h of operation at 200 mA cm^{-2}
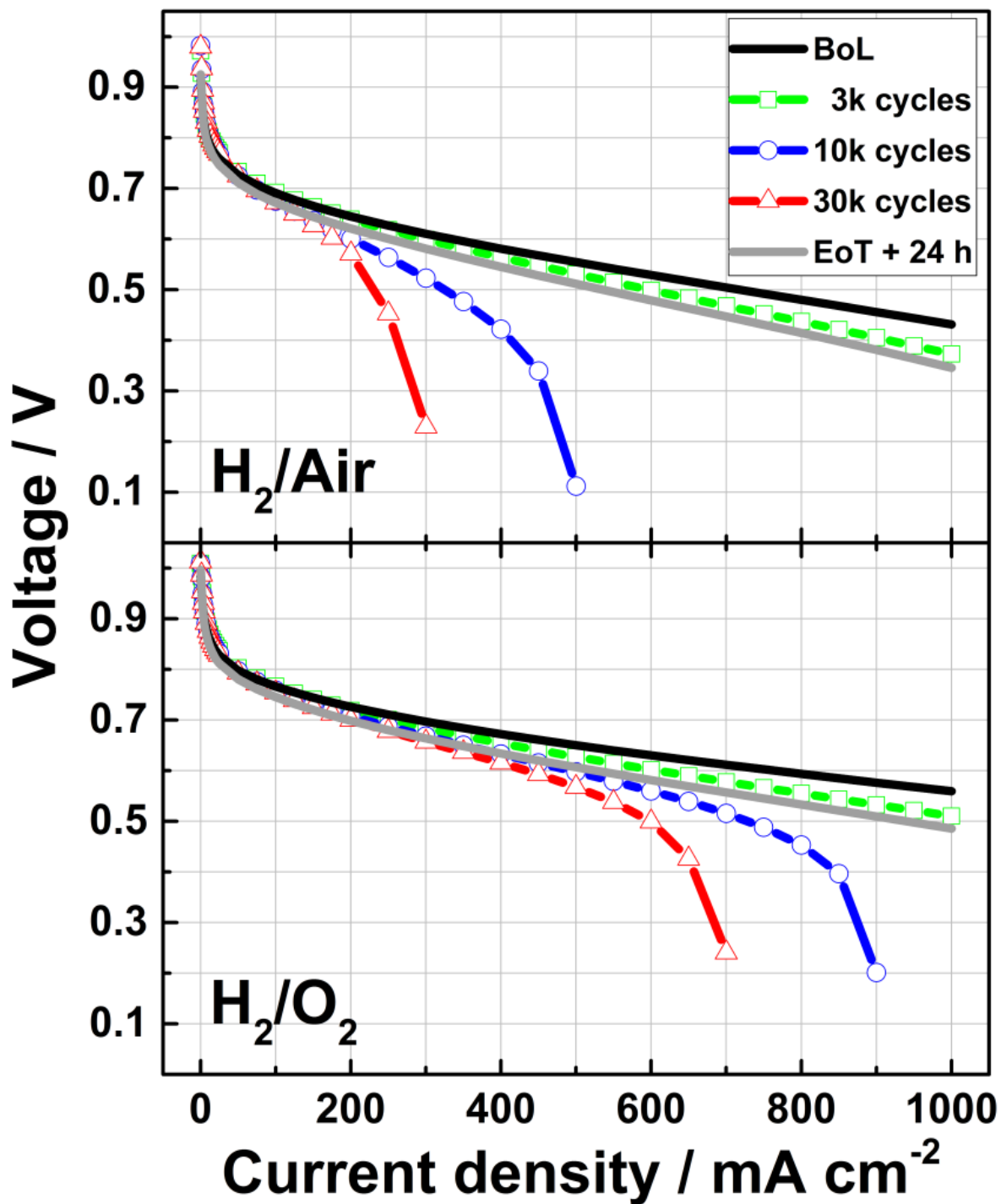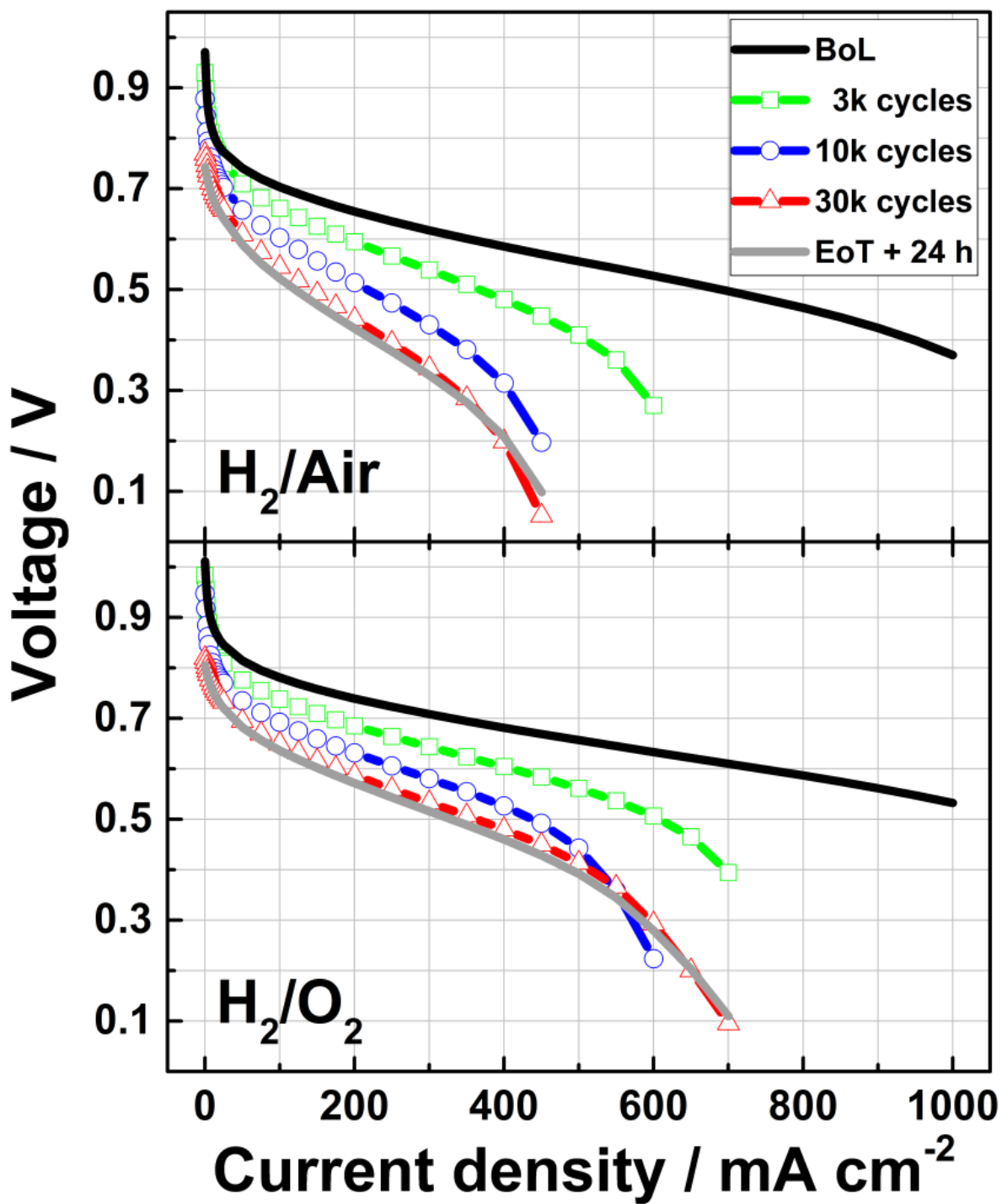
Fig. 3 EIS measurements at BoL, after the specified number of cycles with H_2/N_2 (unhumidified) and also after 30,000 cycles followed by 24 h of operation at 200 mA cm^{-2}
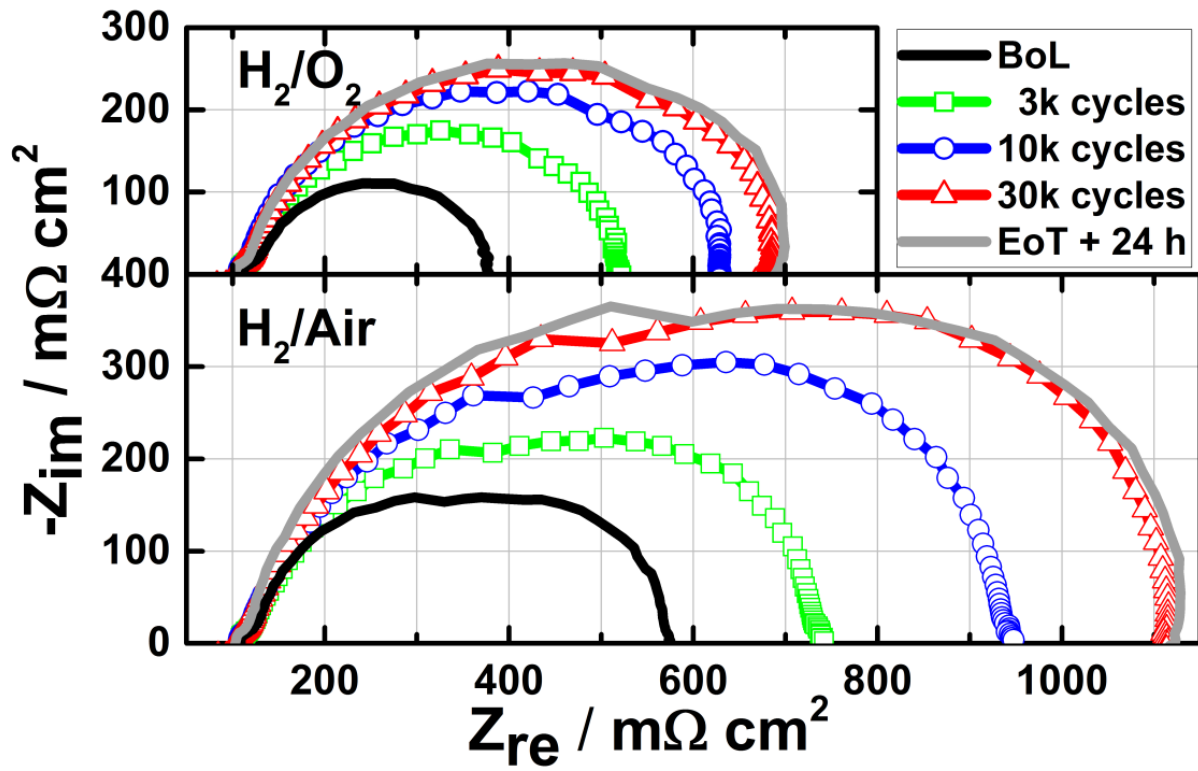
Fig. 4 Polarization characteristics at BoL, after the specified number of cycles with H_2/N_2 (humidified), and also after 30,000 cycles followed by 24 h of operation at 200 mA cm^{-2}

Fig. 5 EIS measurements at BoL, after the specified number of cycles with H_2/N_2 (humidified), and also after 30,000 cycles followed by 24 h of operation at 200 mA cm^{-2}

Fig. 6 OCV from all polarization curves. Measurements were made with either H_2/air or H_2/O_2 after the indicated amount of cycling with either H_2/N_2 (unhumidified) or with H_2/N_2 (humidified)
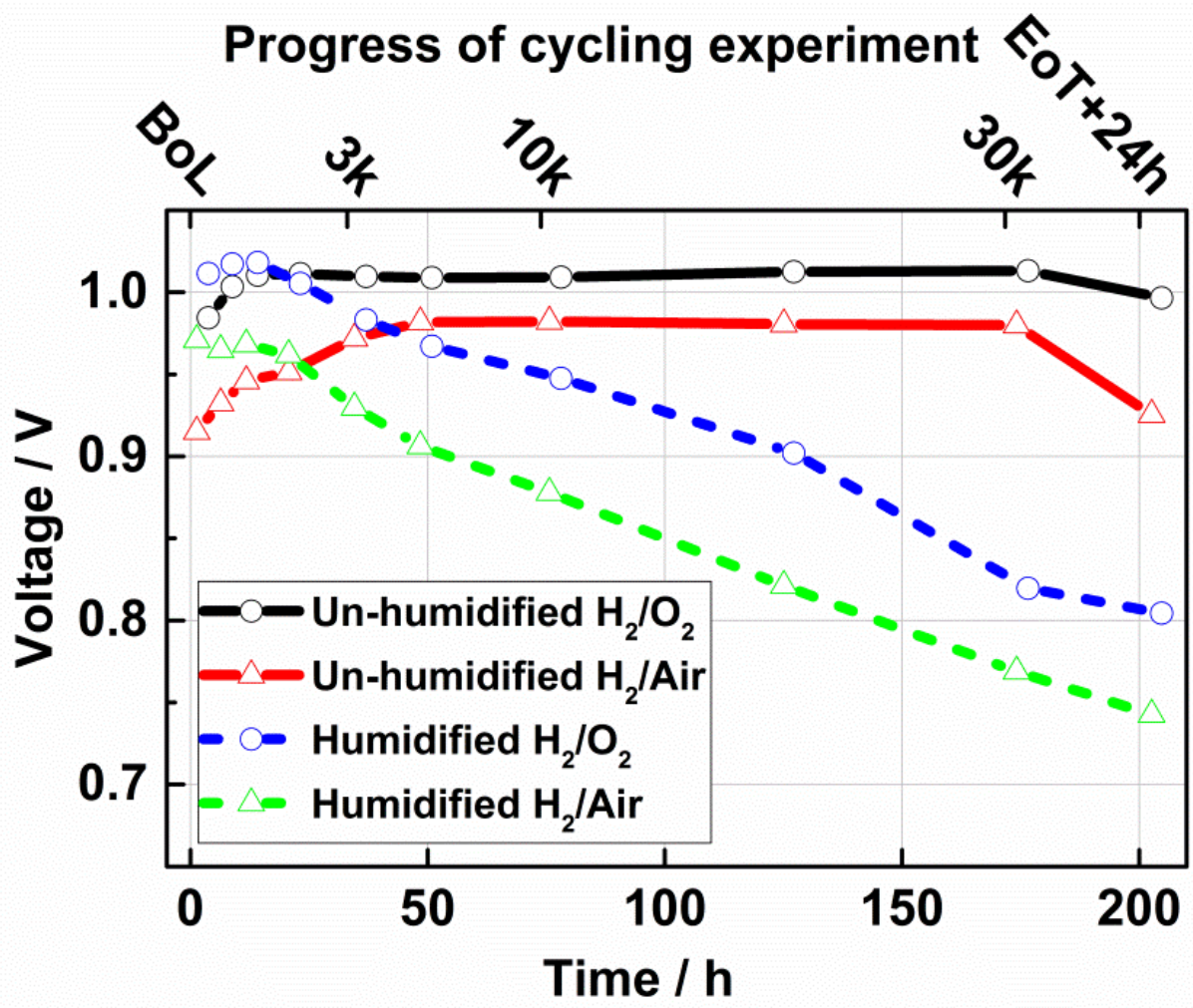
Fig.7 Series resistance from all EIS spectra. Measurements were made with either H_2/air or H_2/O_2 after the indicated amount of cycling with either H_2/N_2 (unhumidified) or with H_2/N_2 (humidified)
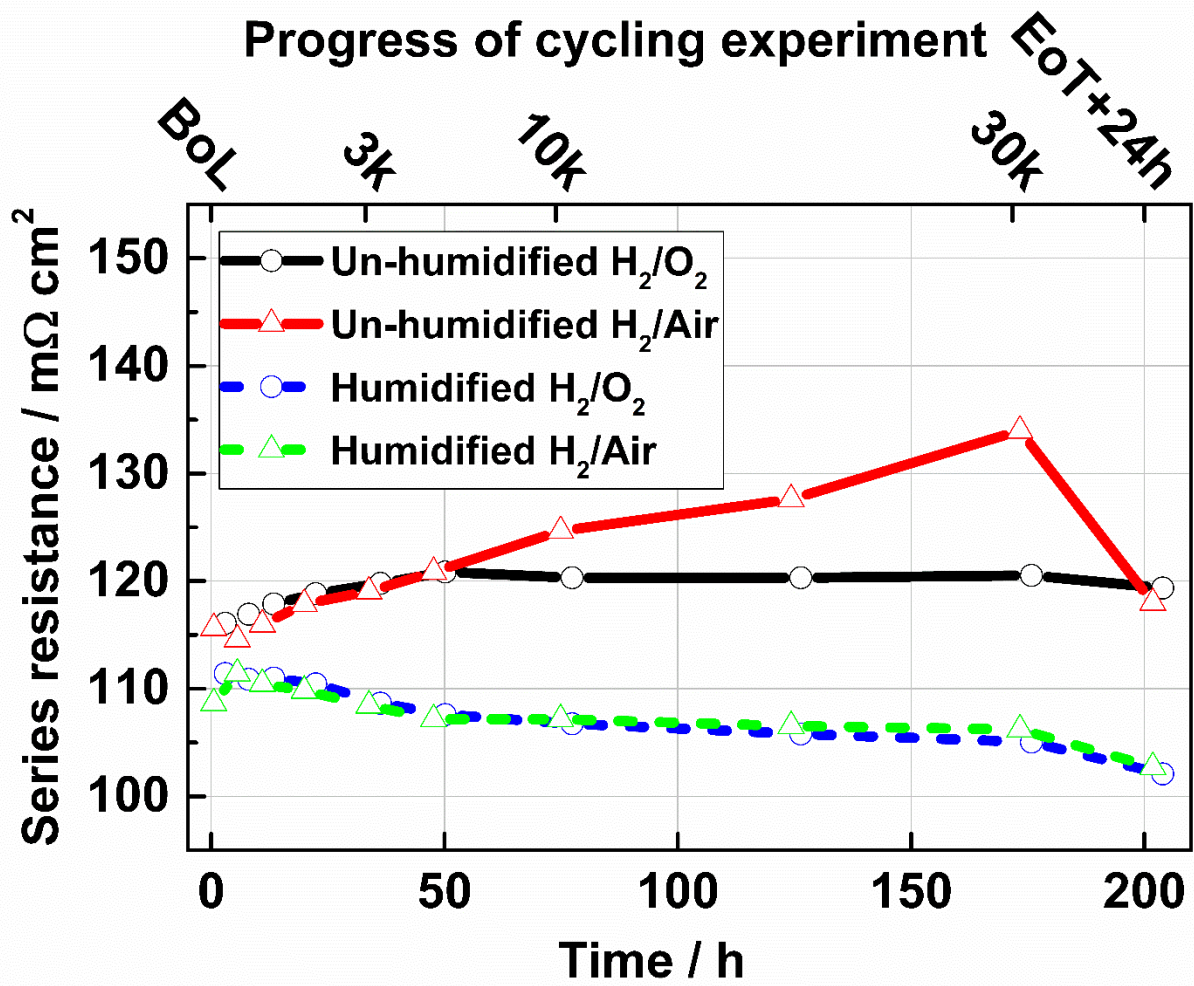
Fig. 8 TEM images of Pt/C catalysts. **a** Pristine catalyst. **b**, **c** The anode after 30,000 cycles with either H_2/N_2 (unhumidified) or with H_2/N_2 (humidified), respectively. **d**, **e** The cathode after 30,000 cycles with either H_2/N_2 (unhumidified) or with H_2/N_2 (humidified), respectively. The colored inserts are histograms of the platinum particle size distribution

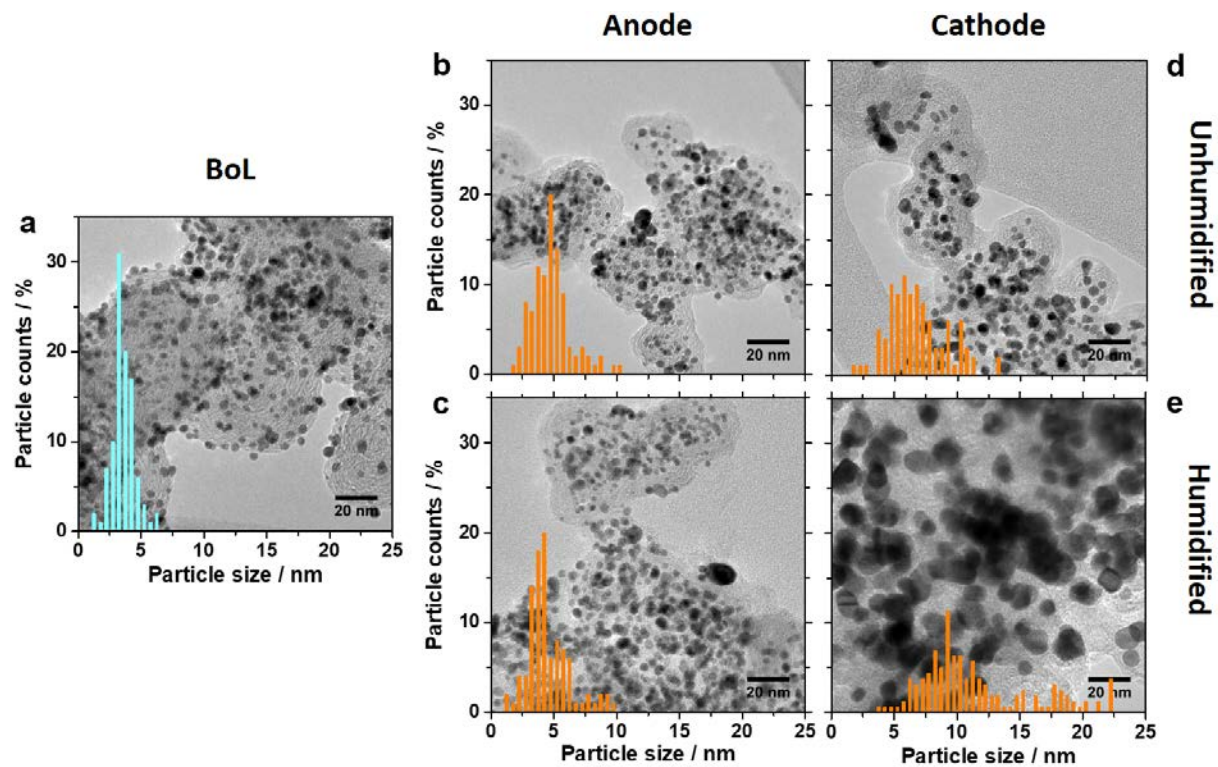**Fig. 9** Cross-sectional backscatter electron images of MEAs after 30,000 cycles. **a** With H_2/N_2 (unhumidified). **b** With H_2/N_2 (humidified). The locations of the EDS line scans are indicated by yellow lines along with the pertaining platinum count profiles in red. The cathode is facing right in both cases